

Prioritized Multi-stream Traffic in Uplink IoT Networks: Spatially Interacting Vacation Queues

Mustafa Emara, *Student Member, IEEE*, Hesham ElSawy, *Senior Member, IEEE*,
Gerhard Bauch, *Fellow, IEEE*

Abstract

Massive Internet of Things (IoT) is foreseen to introduce plethora of applications for a fully connected world. Heterogeneous traffic is envisaged, where packets generated at each IoT device should be differentiated and served according to their priority. This paper develops a novel priority-aware spatiotemporal mathematical model to characterize massive IoT networks with uplink prioritized multi-stream traffic (PMT). Particularly, stochastic geometry is utilized to account for the macroscopic network wide mutual interference between the coexisting IoT devices. Discrete time Markov chains (DTMCs) are employed to track the microscopic evolution of packets within each priority stream at each device. To alleviate the curse of dimensionality, we decompose the prioritized queueing model at each device to a single-queue system with server vacation. To this end, the IoT network with PMT is modeled as spatially interacting vacation queues. Interactions between queues, in terms of the packet departure probabilities, occur due to mutual interference. Service vacations occur to lower priority packets to address higher priority packets. Based on the proposed model, dedicated and shared channel access strategies for different priority classes are presented and compared. The results show that shared access provides better performance when considering the transmission success probability, queues overflow probability and latency.

M. Emara is with the Germany standards R&D team, Next Generation and Standards, Intel Deutschland GmbH and the Institute of Communications, Hamburg University of Technology, Hamburg, 21073 Germany (e-mail: mustafa.emara@intel.com)

H. ElSawy is with the Electrical Engineering Department, King Fahd University of Petroleum and Minerals, 31261 Dhahran, Saudi Arabia (email: hesham.elsawy@kfupm.edu.sa).

G. Bauch is with the Institute of Communications, Hamburg University of Technology, Hamburg, 21073 Germany (email: bauch@tuhh.de).

Index Terms

Internet of Things, spatiotemporal models, priority queues, vacation queues, queueing theory, stochastic geometry, grant-free access

I. INTRODUCTION

New services and vertical market segments are paving the way for a huge market penetration of fifth generation (5G) systems. Emerging segments entail, among other examples, connected vehicles, industrial Internet of Things (IoT), e-health, and smart homes, which are all tied with the IoT technology advancement [1]. To cope with such an evolution, machine type communication (MTC) is defined as a cornerstone for massive IoT deployment over large areas [2]. Third generation partnership project (3GPP) has also introduced the narrowband IoT (NB-IoT) as a low cost solution that utilizes the existing cellular infrastructure to accommodate IoT traffic [3]. The number of non-3GPP IoT commercialized solutions (e.g. LoRaWAN, SigFox and Weightless) are also increasing [4]. In such networks, heterogeneous traffic with different priorities is envisaged. Packets generated at each IoT device should be differentiated and served according to their priority classes. To this end, there is an utter need for mathematical tools to define and assess key performance indicator (KPI)s such as scalability, stability, latency and reliability in the context of massive IoT networks [5].

A. Background

A key enabler of large scale IoT devices is the low cost of deployment, which is realized via distributed and uncoordinated devices [6]. Such a decentralized and low complexity mechanism is achieved in uplink transmissions via grant-free access-based techniques. Accordingly, the scheduling complexity imposed by the scheduling grants from the base stations (BSs) are alleviated, which enables lower latency for critical transmissions [7]. Along with the grant-free uplink communications, the necessity to meet the targeted quality of service (QoS) becomes more prominent with prioritized multi-stream traffic (PMT) and mixed-criticality systems. Devices generate different data streams with diverse priorities. Each stream is characterized by different requirements (e.g. delay and reliability) [8]–[10]. For cellular systems, the concept of QoS class identifier (QCI) was first adopted in long term evolution (LTE) systems to characterize different services and to ensure that resources are allocated appropriately [8]. Each stream (i.e., bearer) has a corresponding QCI, which indicates the service type, priority, packet error rate and packet

delay budget [11]. The presence of such identifiers imposes a different treatment and resource allocation based on their assigned class.

Industrial automation is another sector that relies on PMT, where guaranteed performance regarding successful packet delivery and latency is an imminent KPI [10]. The deployment of wireless-based systems in industrial automation is expected to have diverse requirements for different industrial scenarios (e.g. process and factory automation) [12]. In particular, the IEEE 802.1 time sensitive networking (TSN) task group has been defining amendments that extend the Ethernet protocol with capabilities that enable real-time communication [9]. The IEEE 802.1 Qbv amendment, among its many features, introduces eight different priority classes that are assigned to an incoming traffic streams to define the service requirements of each stream [13], [14]. Accordingly, the presence of such use cases, motivates research towards providing analytical frameworks that aim at deriving key insights on prioritized traffic in massive IoT networks.

Based on the foreseeable massive number of deployed devices, each with its different set of requirements, interference will lead to a deteriorated QoS, thus, hindering delivery of the promised gains. Stochastic geometry is a prominent framework to characterize interference within the large-scale wireless networks [15]–[17]. However, an underlying limiting aspect of the stochastic-geometric models is the full buffer assumption, which assumes that the transmitter has always backlogged packets to be transmitted. Thus, conventional models based on stochastic geometry are oblivious to the temporal domain and the underlying queueing dynamics at each device. To account for the temporal domain, recent efforts have integrated queueing theory with stochastic geometry, which offers a full spatiotemporal characterization for large-scale networks [18]–[22]. In particular, the work in [18] characterizes the delay outage and signal to interference ratio (SIR) for different scheduling schemes for a cellular heterogeneous network. The authors in [19] present a spatiotemporal characterization for grant-free uplink transmissions in IoT network. The work in [19] is extended and compared to scheduled (i.e., grant-based) uplink transmissions in [20]. Analysis for small cell deployment is presented in [21], where the authors show the cell's load and traffic fluctuations on the coverage probability. For ad hoc setup, the work in [22] presents a fine grained spatiotemporal characterization for location-dependent QoS classes in IoT networks. In summary, existing works consider first come first serve (FCFS) discipline, where differentiation among the transmissions is based on their temporal arrival rather than their priority class. In summary, large scale spatiotemporal IoT analytical framework for priority queues is still an open research problem.

B. Contributions

Throughout this work, we provide an analytical framework that entails the macroscopic and microscopic scales of priority-aware uplink large scale IoT networks. For the macroscopic aspect, tools from stochastic geometry are adopted to model the spatial deployment of the devices and their serving BSs. Tools from queueing theory are employed to characterize the microscopic queue evolution per each priority class at each device. Such integrated spatiotemporal models accounts for the interaction arising between the devices (i.e., queues), in terms of the packet departure probabilities, due to mutual interference between the simultaneously active devices. To track the priority class being served at a given time stamp, a two-dimensional Geo/PH/1 discrete time Markov chain (DTMC) is employed for each device, where Geo stands for geometric inter-arrival process and PH stands for the Phase type departure process [23]. In summary, the main contributions of this paper can be summarized as follows:

- Develop a novel, tractable and scalable PMT queueing model for the preemptive priority-aware transmission which overcomes the curse of dimensionality for large number of priority classes.
- Employ a two dimensional Geo/PH/1 DTMC for the queues at every IoT device to account for the inter-class queues interaction.
- Integrate the developed DTMCs within stochastic geometry framework to account for interference based intrinsic interdependency between the macroscopic- and microscopic-scales.
- Compare the performance of dedicated and shared channel access strategies for the different priority classes.
- Present the priority-aware Pareto frontiers that characterize the stability regions for different system parameters.

C. Notation and Organization

Throughout the paper, we adopt the following notation. Matrices and vectors are represented as upper-case and lower-case boldface letters (\mathbf{A} , \mathbf{a}), respectively. $[\mathbf{A}]_{i,j}$ denotes the i -th row and j -th column element of \mathbf{A} , whereas $[\mathbf{A}]_{i,:}$ and $[\mathbf{A}]_{:,j}$ denotes all element in the i -th row and all elements in the j -th column, respectively. The element wise Hadamard product is represented by the operator \odot . The function $\mathcal{Q}([\mathbf{A}]_{i,j}, b)$ replaces the element in the i -th row and j -th column of \mathbf{A} with the scalar b . The indicator function is denoted as $\mathbb{1}_{\{a\}}$ which equals 1 if the expression a is true and 0 otherwise. The $(\cdot)^T$ denotes the transpose operation. All ones and zeros column

vectors of dimension m are represented as $\mathbf{1}_m$ and $\mathbf{0}_m$, respectively. In addition, \mathbf{I}_m and \mathcal{I}_m denote, respectively, the identity and all ones matrices of dimension $m \times m$. The complement operator is denoted by the over-bar (i.e., $\bar{v} = 1 - v$). The notations $\mathbb{P}\{\cdot\}$ and $\mathbb{E}\{\cdot\}$ denote the probability of an event and its expectation.

The rest of the paper is organized as follows. Section II provides the system model and the underlying physical and medium access control (MAC) assumptions. The proposed queueing model along with the microscopic intra-device interactions among the priority queues are presented in Section III. Section IV shows the macroscopic inter-device queueing interactions in terms of mutual interference. Simulation results are presented in Section V. Finally, Section VI summarizes the work and draws some conclusions.

II. SYSTEM MODEL

A. Spatial and Physical Layer Parameters

This work studies a cellular uplink network, where the BSs and IoT devices are spatially deployed in \mathbb{R}^2 according to two independent homogeneous Poisson point processes (PPPs), denoted by Ψ and Φ with intensities λ and μ , respectively. Single antennas are employed at all devices and BSs. As mentioned earlier, grant-free access is assumed, where the devices attempt their transmissions on a randomly selected resource without a scheduling grant from their serving BS. In this paper, a single connectivity is adopted where each device is served by its nearest BS. To alleviate congestion, a set of N_c channels are utilized by the network and a priority-aware random access scheme is adopted by the devices to access the available channels.¹ In particular, we analyze and compare two channel access schemes, namely dedicated and shared channel access. In the former scheme, each priority stream has an exclusive set of channel that can only be accessed by devices to transmit the corresponding priority packets. In the latter scheme, all the channels can be accessed by all devices irrespective of the transmitted packet's priority.

An unbounded path-loss propagation model is adopted such that the signal power attenuates at the rate $r^{-\eta}$, where r is the distance and $\eta > 2$ is the path-loss exponent. Small-scale fading is assumed to be multi-path Rayleigh fading, where the intended and interference channel power

¹This corresponds to the Zadoff-Chu (ZC) codes utilized in LTE and 5G system for the random access channels (RACH) to request a scheduling grants. Similarly, a set of orthogonal resources can be dedicated for IoT devices to directly send their sporadically generated packets.

gains h and g , respectively, are exponentially distributed with unity power gain. All channel gains are assumed to be spatially and temporally independent and identical distributed (i.i.d.). Full channel-inversion power control is adopted, which implies that all devices adjust their transmit powers such that the received uplink average powers at their serving BS is equal to a predetermined value ρ [24]. In this work, a network-wide threshold ρ is assumed for all the devices. A dense deployment of BSs is assumed, ensuring that every device is able to invert its channel almost surely. To this end, a packet generated at a given device is successfully decoded at its serving BS if the received signal to interference noise ratio (SINR) is larger than a predefined threshold θ . In case of successful decoding, that serving BS transmits an ACK through an error-free channel so the device can remove this intended packet from its respective queue. In case of failed decoding, the serving BS sends out a NACK and the packet remains at the head of the device's queue, awaiting a new transmission attempt in the next time slot. During this work, we assume negligible transmission time required for ACK and NACK. To this end, let p_i and TSP_i denote the coverage probability and the transmission success probability (TSP) of the i -th priority queue, respectively, which equal

$$p_i = \mathbb{P}\{\text{SINR}_i > \theta\}, \quad (1)$$

$$\text{TSP}_i = \gamma_i p_i, \quad (2)$$

where γ_i is transmission probability of the i -th priority queue.²

B. MAC Layer Parameters

The proposed framework considers a synchronized, time slotted and priority-aware system, in which packets of different priorities are generated at the existing devices. A PMT model is assumed such that packets are generated at each priority class independently of other classes. Hence, for a system with different N priority classes, batch arrivals up to size N can occur in every time slot. Independent geometric inter-arrival times are assumed between packets belonging to each priority class with parameters $\alpha_i \in [0, 1]$ packet/time slot, where $i \in \{1, 2, \dots, N\}$. Through this work, traffic parameterized with lower indices have higher priority. Without loss

²It is noteworthy to mention that TSP_i depicts the departure probability of a packet residing in the i -th priority queue. It will be shown later through the next sections how does this metric affects the interdependency between the macroscopic and microscopic scales of the network.

of generality, it is reasonable to assume that lower priority packets traffic is generated at higher rates $\alpha_N > \dots > \alpha_i > \dots > \alpha_1$, which complies with the intuition that critical events are rare.

Each device is equipped with a finite queue for each traffic stream, where the i -th priority queue can accommodate up to k_i packets. Generally, we consider that each device has N -priority finite queues that accumulate generated packets according to their tagged priorities. The devices employ a priority-aware transmission scheme that prioritizes the transmission of high priority over lower priority packets³. We assume arrival and departure of packets only occurs at the start of a time slot. If a high priority packet arrives at its respective queue while a lower priority queue is being addressed, service is interrupted and switched to the higher priority queue. The interrupted service is resumed after the high priority queue is empty. Accordingly, we consider an inter-class preemptive discipline along with an FCFS discipline within each priority class [25].

BSs have no knowledge regarding the status of the devices queues. Consequently, the IoT devices employ a random access process to transmit their packets. Only devices with non-empty queues access the channels, where each device attempt to transmit one of its highest priority backlogged packets. For dedicated spectrum access scheme, the device randomly and uniformly selects one of the channels dedicated for the addressed packet priority. For the shared access scheme, the device randomly and uniformly selects one of the complete set of channels regardless of the packet priority. In both cases (i.e., dedicated and shared access) the channel selection process is repeated in each transmission attempt.

Pictorially, a snapshot realization of the network for two priority classes is shown in Fig. 1. The right-hand side of the figure highlights a macroscopic network view and the left-hand side emphasizes the microscopic scale of three links. Due to the adopted preemptive priority discipline, imposed by the priority filter block, packets existing at high priority queues are prioritized for service (i.e., transmission) over packets existing in lower priority queues. Otherwise, the backlogged lower priority packets can be directly served. In the case of having empty queues, no transmission is attempted and the device does not contribute to the network interference. It is worth noting that the time scale of channel fading, packet generation and transmission is much

³This implies that no lower priority packet can be transmitted given that a packet with higher priority exists at the device.

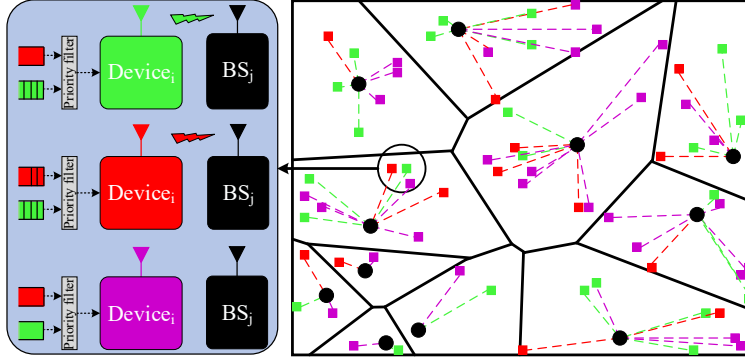


Fig. 1: A snapshot realization of the network with two priority classes. Black circles depicts serving BSs while red and green squares represent devices with first and second priority packets in their queues, respectively. Magenta squares represent devices with no packets in their aggregated queues. The Voronoi cells of the BSs are denoted by the solid black lines while the dashed lines denote the associations of the devices to their serving BSs.

smaller than that of the spatial dynamics.⁴

III. MICROSCOPIC QUEUEING THEORY ANALYSIS

Throughout this section, a novel technique to model the PMT is presented. In order to mathematically describe the different priority classes, the conventional way of characterizing the system is based on the following state space [23, Chapter 9] $\Delta_n = \{(z_{1,n}, z_{2,n}, \dots, z_{N,n}); 0 \leq z_{i,n} \leq k_i; i \in \{1, 2, \dots, N\}\}$, where $z_{i,n}$ denotes the number of packets residing in the i -th priority queue at the n -th time slot. Although tractable for the case of $N \leq 2$, the depicted state space becomes disproportionately complex, causing curse of dimensionality dilemma, when larger values of N are considered. As a result, we seek to introduce a scalable and tractable model for a general number of priority classes based on vacation queues.

A. Vacation Model Motivation & Description

Priority queues can be modeled using vacation queues, where the of the low priority queues takes vacation to serve high priority queues [25]. In other words, the PMT system is decomposed into single-queue vacation systems, where the server is alternatively available and unavailable for a given priority class. The unavailability of the server, denoted as vacation, is due to serving

⁴Accordingly, each spatial network realization for the adopted PPPs remains static over sufficiently large number of time slots, while channel fading, queue states, and device activities change from one time slot to another

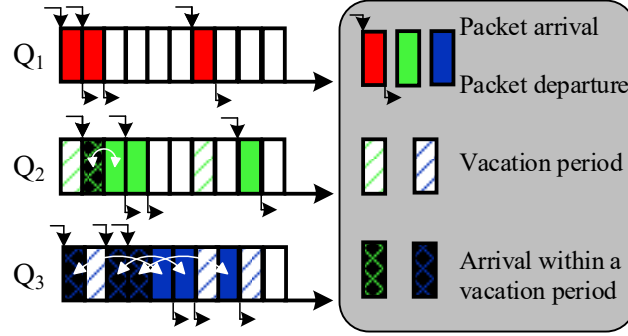


Fig. 2: Vacation-based preemptive priority queues for $i = 3$. Packets for the first, second and third priority classes are depicted by red, green and blue, respectively. White curved arrows represent on-hold property of the lower priority queues.

higher priority packets [26], [27]. An illustrative example for the first three class priorities is shown in Fig. 2. One can observe that the highest priority queue (i.e., Q_1) is agnostic to all the lower priority queues whereas the second queue (i.e., Q_2) will be in vacation till Q_1 is empty. Similarly, Q_3 will be in vacation till the two higher queues are empty. Conceptually, a given queue will go strictly to vacation if a packet resides in any of the higher priority queues. It is noteworthy that for purpose of demonstration, the mentioned figure assumes a hypothetical flawless server (i.e. $p_1 = p_2 = p_3 = 1$), which ignores the events of packet transmission failure due to the aggregate network interference from mutually active devices.

As observed, the vacation period for the i -th queue is the busy periods summation of the higher queues (i.e., Q_m , $m \in \{1, 2, \dots, i-1\}$). Thus, the i -th queue's vacation period can be modeled via PH type distribution, which tracks the server's status whether it is serving the intended (i.e., i -th) priority queue or in vacation, serving higher priority queues. By virtue of preemptive priority, there is no need to track any of the lower priority queues (i.e., Q_m , $m \in \{i+1, \dots, N\}$) when analyzing the i -th priority class.

The state space for the proposed model is characterized as $\Delta_v = (\mathcal{S}_{z_{i,n}}, \mathcal{V}_{(z_{1,n}, z_{2,n}, \dots, z_{i-1,n})})$, where $\mathcal{S}_{z_{i,n}}$ represents the serving state, where the i -th priority queue is addressed at the n -th time slot. In addition, $\mathcal{V}_{(z_{1,n}, z_{2,n}, \dots, z_{i-1,n})}$ captures the vacation state of the i -th queue where it serves any higher priority queues. The server's state can be visualized as shown in Fig. 3 which shows the queues evolution for the case of $i = 3$. A two-dimensional Geo/PH/1 Markov chain is employed to model each IoT device. The horizontal transitions represent the state of the server, denoted as phase, whether in vacation serving higher priority packets or serving the intended i -th priority queue. The vertical transitions represent the number of the packets in the i -th priority

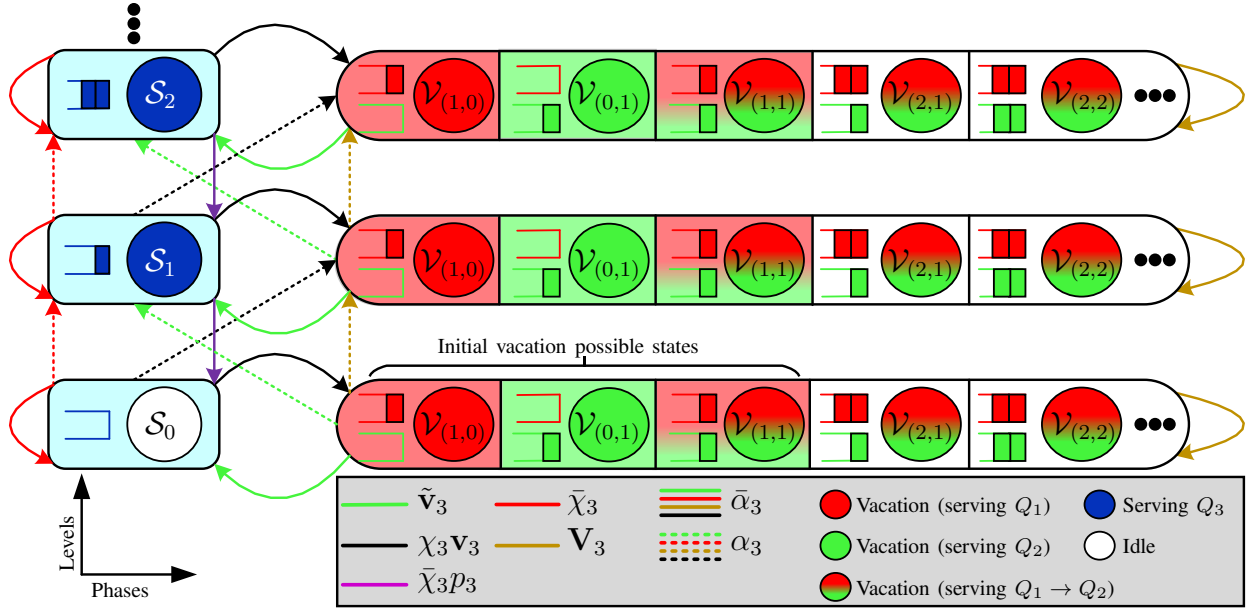


Fig. 3: Two-dimensional discrete-time Markov chain modeling the vacation-based priority queues for $i = 3$. States for the first, second and third priority classes are depicted by red, green and blue circles, respectively. The white highlighted state represents the idle state, where all queues are empty. Possible initial states for the construction of \mathbf{v}_3 are highlighted. Solid (dashed) lines are all multiplied by $\bar{\alpha}_3$ (α_3).

queue, denoted as levels.

The PH type distribution of the server vacation is represented via an absorbing Markov chain. That is, when serving higher priority packets, the server will be looping in the transient states of the PH type distribution. The state of absorption shows that the server came back from vacation, which occurs when all higher priority packets are served and their corresponding queues are empty. Absorbing Markov chain are mathematically described via an initialization vector and a transient matrix. In our case, the initialization vector and transient matrix are denoted as \mathbf{v}_i and \mathbf{V}_i , respectively. The initialization vector \mathbf{v}_i captures all the possible initial states for vacations with their corresponding probabilities. That is, any combination of batch arrivals that include higher priority packets represents a legitimate initial state for the server vacation. For $i = 3$, all legitimate initial states for vacation with two higher priority classes are illustrated in Fig. 3. The transient matrix \mathbf{V}_i tracks the server vacation through tracking the temporal evolution (i.e., arrivals and departures) of packets in higher priority queues. Adopting such vacation-based model allows a systematic and scalable approach to model a generic N -priority queues.

where $\mathbf{B}_{1,i}$, \mathbf{C}_i and $\mathbf{B}_{2,i} \in \mathbb{R}^{m_i \times m_i}$ are the boundary sub-stochastic matrices. In addition, $\mathbf{A}_{0,i}$, $\mathbf{A}_{1,i}$ and $\mathbf{A}_{2,i} \in \mathbb{R}^{m_i \times m_i}$ represent the sub-stochastic matrices that capture the transition down a level, up a level, and in a fixed level within the QBD, respectively.

In details, $\mathbf{B}_{1,i}$ captures the case where all the queues are empty (i.e., white-shaded state in Fig. 3). It can be computed based on the PH type distribution as $\mathbf{B}_{1,i} = \bar{\alpha}_i \mathbf{S}_{0,i}$, where $\mathbf{S}_{0,i}$ is the stochastic transient boundary matrix. Similarly, \mathbf{C}_i captures the transition to level 1, that represents an increment of the i -th priority packets and is computed as $\mathbf{C}_i = \alpha_i \mathbf{S}_{0,i}$. The forward transitions sub-matrix $\mathbf{A}_{0,i} = \alpha_i \mathbf{S}_i$ represents the case where a new packet arrives and no packet departs (i.e., vacation state or serving state with transmission failure). The local transitions sub-matrix $\mathbf{A}_{1,i} = \alpha_i \mathbf{s}_i \boldsymbol{\beta}_i + \bar{\alpha}_i \mathbf{S}_i$ represents no packet arrival while in transient state or a simultaneous arrival of one packet and a departure of another packet of the same priority (i.e., horizontal transitions in Fig. 3). The backward transitions sub-matrix $\mathbf{A}_{2,i} = \bar{\alpha}_i \mathbf{s}_i \boldsymbol{\beta}_i$ captures the case of a packet being dispatched while in serving state, leading to a decrement of the i -th queue packets. Finally, the boundary sub-matrix $\mathbf{B}_{2,i} = \alpha_i \mathbf{s}_i \boldsymbol{\beta}_i + \mathbf{S}_i$ captures the events when the i -th queue is full. Note that packets of the i -th priority that arrive in this state are lost due to queue overflow. Due to the embedded (i.e., two level) vacation model employed, a packet departure implies that the server is available. Hence, the initialization vector of $\boldsymbol{\beta}_i = [1 \ \mathbf{0}_{m_i-1}]^T$ has only 1 at the serving state and zeros otherwise.

In order to construct the QBD via (5), the stochastic transient matrices \mathbf{S}_i , $\mathbf{S}_{0,i}$ are required. We first present preliminary definitions that facilitate the characterization of $\mathbf{S}_{0,i}$ and \mathbf{S}_i . Let χ_i denote the probability that the i -th queue server starts a vacation. Due to the adopted preemptive priority discipline, a vacation starts upon the arrival of any of the higher priority packets. Exploiting the independence between all arrival streams, χ_i is given by

$$\chi_i = 1 - \prod_{m=1}^{i-1} \bar{\alpha}_m. \quad (6)$$

Let $\mathbf{v}_i \in \mathbb{R}^{1 \times m_i-1}$ denotes the vacation initialization vector, which have only non-zero values at the legitimate initial vacation states (i.e., highlighted in Fig. 3 for $i = 3$). The two level PH type distribution used to construct QBD in (5) is characterized through the following lemma

Lemma 1. *The stochastic transient matrices of the i -th priority class with coverage probability*

p_i , for the boundary and non-boundary states $\mathbf{S}_{0,i}$ and \mathbf{S}_i , respectively, depend on $\tilde{\mathbf{S}}_i$ as follows

$$\mathbf{S}_{0,i} = \tilde{\mathbf{S}}_i \quad (7)$$

$$\mathbf{S}_i = \tilde{\mathbf{S}}_i \odot \mathcal{Q}([\mathcal{I}_{m_i}]_{1,1}, \bar{p}_i), \quad (8)$$

where $\tilde{\mathbf{S}}_i$ is defined as

$$\tilde{\mathbf{S}}_i = \begin{bmatrix} \bar{\chi}_i & \chi_i \mathbf{V}_i \\ \tilde{\mathbf{v}}_i & \mathbf{V}_i \end{bmatrix}. \quad (9)$$

$\mathbf{V}_i \in \mathbb{R}^{m_i-1 \times m_i-1}$ is the vacation visit matrix which equals $\mathbf{V}_i = \mathbf{D}_i \mathbf{P}_i \mathbf{D}_i^T$ where the selection matrix $\mathbf{D}_i = [\mathbf{0}_{m_i-1} \quad \mathbf{I}_{m_i-1}]$. The absorption vector is computed as $\tilde{\mathbf{v}}_i = \mathbf{1}_{m_i-1} - \mathbf{V}_i \mathbf{1}_{m_i-1}$.

Proof. See Appendix A ■

It is clear from (9) that the transient matrices $\mathbf{S}_{0,i}$ and \mathbf{S}_i encompass all vacation phases in \mathbf{V}_i along with the serving phase entered through the absorbing vector $\tilde{\mathbf{v}}_i$ and departed via the probability vector $\chi_i \mathbf{V}_i$.

Once the PH type distribution is constructed, the steady state distribution of each priority queue at each device can be computed. Let $\mathbf{A}_i = \mathbf{A}_{0,i} + \mathbf{A}_{1,i} + \mathbf{A}_{2,i}$ and let π_i represent the unique solution of $\pi_i \mathbf{A}_i = \pi_i$, with the normalization condition $\pi_i \mathbf{1}_{m_i} = 1$. Since finite queues are considered at the devices, one is interested to determine the critical arrival rate after which the probability of having full queues starts to dominate and the queues tends to be always non-empty [29]. Through the rest of the paper, we use the term overflow (non-overflow) region to denote operating beyond (below) such a rate. Mathematically, for the DTMC in (5) to be in the non-overflow region, the following condition must be satisfied⁵

$$\pi_i \mathbf{A}_{2,i} \mathbf{1}_{m_i} > \pi_i \mathbf{A}_{0,i} \mathbf{1}_{m_i}. \quad (10)$$

Let $\mathbf{x}_i = [\mathbf{x}_{i,0} \quad \mathbf{x}_{i,1} \quad \cdots \quad \mathbf{x}_{i,k_i}]$ be the steady state probability vector characterizing the i -th queue, where $\mathbf{x}_{i,j}$ denotes the probability of having j packets in the i -th queue which equals $\mathbf{x}_{i,j} = [x_{(1,z_1),(2,z_2),\dots,(i-1,z_{i-1}),(i,j)}]$, $\forall z_m \in \{0, 1, 2, \dots, k_m\}$ and $m \in \{1, 2, \dots, i-1\}$. The scalar $x_{(1,z_1),(2,z_2),\dots,(i-1,z_{i-1}),(i,j)}$ denotes the joint probability of having $z_1, z_2, \dots, z_{i-1}, j$ packets in the first, second, ..., $i-1$ and i -th queues, respectively. With a little abuse of notation, $\mathbf{x}_{i,j}$ represents vector of the i -th queue having j packets considering all possible combinations of

⁵It is important to note that if the condition in (10) is not satisfied, the probability of having full queues starts to dominate even with larger queue sizes.

the higher priority queue states. On the other hand, $x_{i,j}$ represents the probability of all such possible combinations. Based the employed vacation model, $x_{i,j}$ equals

$$x_{i,j} = \sum_{z_1=0}^{k_1} \sum_{z_2=0}^{k_2} \cdots \sum_{z_{i-1}=0}^{k_{i-1}} x_{(1,z_1),(2,z_2),\dots,(i-1,z_{i-1}),(i,j)}. \quad (11)$$

Observing Fig. 2, the third priority queue is only granted service (i.e. transmission attempt) when the higher queues are idle. The transmission probability γ_i can be computed as

$$\gamma_i = \sum_{z_i=0}^{k_i} x_{(1,0),(2,0),\dots,(i-1,0),(i,z_i)}, \quad (12)$$

whereas for the first priority class $\gamma_1 = 1$. Let $r_i = m_i(k_i + 1)$ be the number of possible states for the i -th queue, then the steady state solution for a stable system can be computed as follows

Lemma 2. *The steady state distribution for the i -th queue with state transition matrix \mathbf{P}_i is*

$$\mathbf{x}_i = \mathbf{1}_{r_i}^T (\mathbf{P}_i - \mathbf{I}_{r_i} + \mathcal{I}_{r_i})^{-1}. \quad (13)$$

Proof. Since we are considering finite DTMC based on (5), the steady state vector \mathbf{x}_i satisfies

$$\mathbf{x}_i \mathbf{P}_i = \mathbf{x}_i, \quad \mathbf{x}_i \mathbf{1}_{r_i} = 1, \quad (14)$$

which is a classical linear algebra problem of the form $\mathbf{A}\mathbf{x} = \mathbf{b}$, and employing [30, Lemma 1], the lemma can be proved. ■

C. Alternative Computationally Convenient Solution

The mathematical complexity required for the inversion in (13) can be cumbersome, specially for large number of priority classes and large queue sizes k_i . Thus, a less-complex and mathematically tractable solution is sought as an alternative way to solve the DTMC employed at each device. The matrix analytic method (MAM) is a powerful mathematical tool which is most suited to Markov chains with QBD structure [28], [23]. Based on the state transition matrix defined in (5), the following lemma derives the steady state distribution for the i -th priority queue.

Lemma 3. *The steady state distribution based on the MAM for the i -th queue is*

$$\mathbf{x}_{i,j} = \begin{cases} \Upsilon_i \mathbf{A}_{2,i} (\mathbf{I}_{m_i} - \mathbf{B}_{1,i})^{-1}, & j = 0, \\ \Upsilon_i, & j = 1, \\ \mathbf{x}_{i,1} \mathbf{R}_i^{j-1}, & j > 1, \end{cases} \quad (15)$$

where $\Upsilon_i = \mathbf{x}_{i,0} \mathbf{C}_i (\mathbf{I}_{m_i} - \mathbf{A}_{1,i} - \mathbf{R}_i \mathbf{A}_{2,i})^{-1}$ and \mathbf{R}_i is the MAM matrix and is given by $\mathbf{R}_i = \mathbf{A}_{0,i} (\mathbf{I}_{m_i} - \mathbf{A}_{1,i} - \mathbf{A}_{0,i} \boldsymbol{\beta}_i)^{-1}$. In addition, (15) must satisfy the normalization $\mathbf{x}_{i,0} \mathbf{1}_{m_i} + \Upsilon_i (\mathbf{I}_{m_i} - \mathbf{R}_i)^{-1} \mathbf{1}_{m_i} = 1$.

Proof. Based on [28], [23], \mathbf{R}_i is the minimal non-negative solution to the quadratic equation $\mathbf{R}_i = \mathbf{A}_{0,i} + \mathbf{A}_{1,i} + \mathbf{A}_{2,i}$. Let $\mathbf{x}_{i,0}$ and $\mathbf{x}_{i,1}$ be the solution to

$$\begin{bmatrix} \mathbf{x}_{i,0} & \mathbf{x}_{i,1} \end{bmatrix} = \begin{bmatrix} \mathbf{x}_{i,0} & \mathbf{x}_{i,1} \end{bmatrix} \begin{bmatrix} \mathbf{B}_{1,i} & \mathbf{C}_i \\ \mathbf{A}_{2,i} & \mathbf{A}_{1,i} + \mathbf{R}_i \mathbf{A}_{2,i} \end{bmatrix}. \quad (16)$$

The employed DTMC has an advantageous feature that can be exploited, since $\mathbf{A}_{2,i}$ is a rank one matrix, which simplifies \mathbf{R}_i to

$$\mathbf{R}_i = \alpha_i \mathbf{S}_i (\mathbf{I}_{m_i} - \bar{\alpha}_i \mathbf{s}_i \boldsymbol{\beta}_i - \bar{\alpha}_i \mathbf{S}_i - \alpha_i \mathbf{S}_i \mathbf{1}_{m_i} \boldsymbol{\beta}_i). \quad (17)$$

Given that (10) is satisfied, \mathbf{R}_i has a spectral radius less than one [23]. The solution to (16) is expressed as

$$\begin{aligned} \mathbf{x}_{i,0} &= \alpha_i \mathbf{x}_{i,0} \mathbf{S}_0 (\mathbf{I}_{m_i} - \alpha_i \mathbf{s}_i \boldsymbol{\beta}_i - \bar{\alpha}_i \mathbf{S}_i - \mathbf{R}_i \bar{\alpha}_i \mathbf{s}_i \boldsymbol{\beta}_i)^{-1} \\ &\quad \bar{\alpha}_i \mathbf{s}_i \boldsymbol{\beta}_i (\mathbf{I}_{m_i} - \bar{\alpha}_i \mathbf{S}_0)^{-1}, \end{aligned} \quad (18)$$

with the normalization $\mathbf{x}_{i,0} \mathbf{1}_{m_i} + \alpha_i \mathbf{x}_{i,0} \mathbf{S}_0 (\mathbf{I}_{m_i} - \alpha_i \mathbf{s}_i \boldsymbol{\beta}_i - \bar{\alpha}_i \mathbf{S}_i - \mathbf{R}_i \bar{\alpha}_i \mathbf{s}_i \boldsymbol{\beta}_i)^{-1} (\mathbf{I}_{m_i} - \mathbf{R}_i)^{-1} \mathbf{1}_{m_i} = 1$. Finally, $\mathbf{x}_{i,1}$ is obtained through solving (16) and $\mathbf{x}_{i,j} = \mathbf{x}_{i,1} \mathbf{R}^{-1}$. Substituting the component stochastic matrices, the lemma can be reached. \blacksquare

D. Vacation Model Verification

As verification, the proposed vacation-based preemptive model is compared against the conventional method presented in [23, Chapter 9] for the case of $N = 2$. Assuming a hypothetical fixed service probability p_i^6 , Fig. 4 compares the conventional method with the proposed one. It is observed that the vacation-based model perfectly characterizes the priority queues evolution while offering a computationally convenient, tractable, and scalable model for larger number of priority classes. For higher values of N , the conventional method becomes highly complex.

Finally, it is clear that in order to compute the steady state distributions x_i of the i -th queue, one need to compute p_i . Such a dependency highlights the interaction between microscopic and macroscopic scales in the network. In what follows, we present the framework adopted to characterize p_i based on stochastic geometry analysis.

⁶The true value of p_i is calculated in Section IV via stochastic geometry analysis

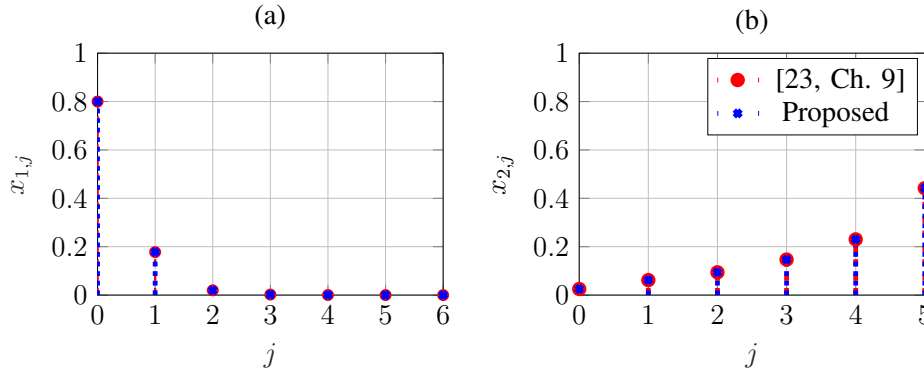


Fig. 4: Steady state distribution for (a) first (b) second priority class comparing the scheme in [23] with the proposed model for $k_1 = 6, k_2 = 5, \alpha_1 = 0.1, \alpha_2 = 0.5$ and $p_1 = p_2 = 0.5$.

IV. MACROSCOPIC LARGE SCALE ANALYSIS

The queueing analysis in Section III requires the coverage probability p_i (i.e., the probability of successful transmission attempt) defined in (1). In particular, Lemma 1 requires p_i in (8) to construct the PH type distribution of the developed queueing model. From the definition in (1), it is clear that the p_i is a function of the aggregate network interference induced by the macroscopic interactions between the devices. This section utilizes stochastic geometry to delve into the network-wide interactions between devices and characterizes the coverage probability in (1). Before proceeding further, we state two commonly used and core approximations that are utilized in this paper for tractability and mathematical convenience.

Approximation 1. *The spatial correlations between adjacent Voronoi cell areas are ignored.*

Remark 1. *Approximation 1 implies that all devices will have independent and identically distributed transmit powers to invert their path-loss to the serving BS. Such assumption is commonly used and verified in the literature [24], [31].*

Approximation 2. *All devices in the networks are assumed to perform (i.e., in terms of coverage probability) as the typical device located at the origin.*

Remark 2. *In the general case of static networks, the coverage probability is location dependent. Such location dependence is captured via the meta distribution [32] and can be incorporated to the spatiotemporal analysis as in [21], [22]. However, it is shown [19], [20], [33], [34] that such location dependence diminishes with power control and random channel selection. Approximation 1 is based on the reported results in [19], [20], [33], [34] and is introduced for*

the ease of mathematical treatise.⁷

Exploiting Approximation 2 along with Slivnyak Theorem's [35], the coverage probability of a packet belonging to the i -th priority class transmitted from any IoT device in the network, as shown in (1), can be further expressed as

$$p_i = \mathbb{P}\left\{\frac{\rho h_o}{I_i + \sigma^2} \geq \theta\right\}, \quad (19)$$

where $\|\cdot\|$ is the Euclidean norm, h_o is the serving channel gain, σ^2 is the noise power, z_o is the serving BS's location of the typical device, and I_i is the aggregate interference seen by a packet of priority i . The interference term I_i is given by

$$I_i = \sum_{y_j \in \Phi \setminus y_o} \mathbb{1}_{\{a_{i,j}\}} P_j g_j \|y_j - z_o\|^{-\eta} \quad (20)$$

where y_j is the location of an IoT device in the network excluding the intended device $\Phi \setminus y_o$, P_j is its transmit power, g_j is the channel power gain between the interfering device and the intended BS, and $a_{i,j}$ is the event that the device located at y_j is transmitting on the same channel as the intended packet.

Remark 3. *It is worth noting that p_i will only be different for the dedicated spectrum access, where the channel selection is dependent on the packet priority. Hence, a device sending a packet of priority i may only experience interference from devices transmitting packets of the same priority. However, for the case of shared spectrum access, the coverage probability is independent from the packets priorities.*

Due to the assumed exponential distribution of h_o , the channel inversion power control and the definition of the Laplace transform (LT), (19) can be rewritten as

$$p_i = \exp\left\{-\frac{\sigma^2 \theta}{\rho}\right\} \mathcal{L}_{I_i}\left(\frac{\theta}{\rho}\right), \quad (21)$$

where $\mathcal{L}_{I_i}(\cdot)$ is the LT of the aggregate interference I_i . One can observe from (21) the effect of the fading, power control and SINR threshold on the achieved transmission probabilities, which in return affects the employed queues evolution at the device. This leads to the coupled interactions between the queues departure probabilities and the aggregate interference in the network. In the remaining of this section, we characterize the coverage probability for the two different channel access strategies.

⁷Both approximations are validated in Section V against independent Monte Carlo simulations.

A. Dedicated access

The dedicated scheme considers an orthogonal access among the active queues based on their priority class. The interfering sources to an active transmission of the i -th queue can only be from the set of all active devices having packets to be transmitted in their i -th queue. Next, the coverage probability of an i -th priority packet under the dedicated access is derived.

Theorem 1. *The coverage probability p_i of a packet belonging to the i -th priority class under the dedicated access strategy is given by*

$$p_i \approx \frac{\exp \left\{ -\frac{\sigma^2 \theta}{\rho} - \frac{2\theta \zeta_i \kappa_i}{(\eta-2)} {}_2F_1(1, 1 - 2/\eta, 2 - 2/\eta, -\theta) \right\}}{\left(1 + \frac{\theta \zeta_i \kappa_i}{(1+\theta)c} \right)^c}$$

$$\stackrel{(\eta=4)}{=} \frac{\exp \left\{ -\frac{\sigma^2 \theta}{\rho} - \zeta_i \kappa_i \sqrt{\theta} \arctan(\sqrt{\theta}) \right\}}{\left(1 + \frac{\theta \zeta_i \kappa_i}{(1+\theta)c} \right)^c}, \quad (22)$$

where $\zeta_i = \sum_{z_i=1}^{k_i} x_{(1,0),(2,0),\dots,(i-1,0),(i,z_i)}$ is the joint probability of having idle higher priority queues ($1 \leq j \leq i-1$) queues and non-idle i -th queue, $\kappa_i = \frac{\mu}{\lambda N c_i}$ is the average number of devices per BS per channel, ${}_2F_1(\cdot)$ is the Gaussian hypergeometric function and $c = 3.575$. The approximation is due to the employed approximate PDF of the PPP Voronoi cell area in \mathbb{R}^2 .

Proof. See Appendix B ■

The parameter $\kappa_i \zeta_i$ provides the intensity of devices that are transmitting a packet of the i -th priority and selected the same channel as the intended i -th priority packet. Moreover, κ_i is affected by the number of channels assigned to each priority class $N c_i$. Through this work, we investigate two allocation techniques; namely, equal allocation (EA) and weighted allocation (WA). The former considers an equal allocation of the total available channels among the existing priority classes, whereas the latter considers an allocation of channels that is dependent on that given priority class arrival rate. Mathematically, the number of allocated channels for the equal and weighted schemes can be written as

$$N c_i^{\text{EA}} = \frac{N c}{N}, \quad (23)$$

$$N c_i^{\text{WA}} = N c \frac{\alpha_i}{\sum_{j=1}^N \alpha_j}. \quad (24)$$

B. Shared access

This strategy considers the case of inter-class channel multiplexing among all the active devices irrespective of the packet's priority that is to be transmitted. That is, all the active devices can mutually interfere together regardless of the priority of the packets being transmitted. Hence, all the devices with non-empty queues are potential interferers to the intended packet. Recalling the preemptive-based mechanism (c.f. Fig. 2), the probability of being a potential interferer is calculated through the joint idle probability $x_{(1:N,0)}$ of all the N priority queues. In the following theorem, the coverage probability of an i -th priority packet under the shared access is derived.

Theorem 2. *The coverage probability p_i of a packet belonging to the i -th priority class under the shared access strategy is given by*

$$p_i \approx \frac{\exp \left\{ -\frac{\sigma^2 \theta}{\rho} - \frac{2\theta \bar{x}_{(1:N,0)} \kappa}{(\eta-2)} {}_2F_1(1, 1 - 2/\eta, 2 - 2/\eta, -\theta) \right\}}{\left(1 + \frac{\theta \bar{x}_{(1:N,0)} \kappa}{(1+\theta)^c} \right)^c} \\ (\eta \equiv 4) \frac{\exp \left\{ -\frac{\sigma^2 \theta}{\rho} - \bar{x}_{(1:N,0)} \kappa \sqrt{\theta} \arctan(\sqrt{\theta}) \right\}}{\left(1 + \frac{\theta \bar{x}_{(1:N,0)} \kappa}{(1+\theta)^c} \right)^c}, \quad (25)$$

where $x_{(1:N,0)} = x_{(1,0),(2,0),\dots,(N-1,0),(N,0)}$ is the joint idle probability of having all the queues empty and $\kappa = \frac{\mu}{\lambda N_c}$ is the average number of devices per BS per channel.

Proof. See Appendix C ■

In Section V, we will assess and compare the shared, EA and WA access schemes. The shared access scheme allows inter-priority class interference along with a larger number of available channels compared to the dedicated schemes. On the other hand, the dedicated schemes provide interference-protection from the other priority classes, with the cost of lower number of channels, thus, higher intra-priority class interference.

C. Iterative Solution

Based on Lemmas 2 and 1, the idle probability of an i -th priority queue employed at a given IoT device governs the interference it causes to other active devices. Concurrently, the aggregate network interference affect the idle probability of each device. Thus, the interdependency is observed between the microscopic (devices activity) and macroscopic (aggregate interference) scales. Such interdependency can be solved iteratively as presented in Algorithm 1, which converges uniquely to a solution by virtue of fixed point theorem [36].

Algorithm 1 Iterative computation of p_i and \mathbf{x}_i for dedicated and shared access

Input ($\alpha = [\alpha_1 \ \alpha_2 \ \dots \ \alpha_N], \lambda, \mu, \eta, \theta, N_c, \epsilon$)

initialize $x_{(1:N,0)}$, & $\zeta_i \in [0, 1]$

while $\|\mathbf{x}_i^k - \mathbf{x}_i^{k-1}\| \geq \epsilon$ **do**

 Compute p_i from (22)-dedicated or (25)-shared

 Construct $\mathbf{S}_{0,i}$ and \mathbf{S}_i as Lemma 1

if $\pi_i \mathbf{A}_{2,i} \mathbf{1} > \pi_i \mathbf{A}_{0,i} \mathbf{1}$ **then**

 Solve \mathbf{x}_i based on Lemma 2 or Lemma 3

 Compute $x_{(1:N,0)}$ and ζ_i based on \mathbf{x}_i

 Compute p_i from (22)-dedicated or (25)-shared

else

 Set $x_{(1:N,0)} = 0$ and calculate ζ_i

 Compute p_i from (22)-dedicated or (25)-shared

 Break

end if

 Increment k

end while

Output: p_i and $\mathbf{x}_i \forall i$

end Input

D. Performance Metrics

Based on the provided iterative framework, the steady state distribution of each queue belonging to one of the N priority classes is computed. Accordingly, a number of KPIs can be evaluated, which are insightful when designing and assessing massive PMT IoT networks. First, the transmission success probability given by

$$\text{TSP}_i = \gamma_i p_i, \quad (26)$$

where γ_i , defined in (12), is the probability that server is available to serve the i -th priority packet. Articulated differently, γ_i is the probability that all high priority queues are empty such that the device is able to send a packet belonging to the i -th priority class. Such transmission attempt succeeds with probability p_i given by (22) for the dedicated access and (25) for shared access.

Additionally, let Q_i be the instantaneous number of packets at the i -th queue, then the average number of packets is

$$\mathbb{E}[Q_i] = \sum_{n=0}^{k_i} n \mathbb{P}\{Q_i = n\} = \sum_{n=1}^{k_i} n x_{i,n}. \quad (27)$$

Based on the considered PH type distribution for the vacation durations, let W_i be the number of time slots spent in the queue before the service starts for a randomly chosen packet. Averaging over all packets, the expected transmission waiting time can be computed as [23, Section 2.5.3]

$$\mathbb{E}[W_i] = \beta_i (\mathbf{I}_{m_i} - \mathbf{S}_i)^{-1}. \quad (28)$$

For the i -th priority packet residing in its respective queue, its service will be postponed till all the packets belonging to the higher classes are successfully served. In this work, service availability for the i -th priority class in a generic device denotes the probability that the i -th priority queue is non-empty and that all higher priority queues are empty. Thus, service availability is considered an important KPI for prioritized-based transmissions, which is calculated as

$$\mathcal{A}_i = 1 - \sum_{j=1}^{i-1} \sum_{m_j=1}^{k_j} x_{j,m_j} \quad (29)$$

V. SIMULATION RESULTS

Through this section various numerical results are presented that aim at (a) validating the proposed analytical model, (b) highlighting the influence of the access strategies, and (c) showing priority-aware wireless-based system design insights.

A. Simulation Methodology

The developed simulation framework incorporates microscopic and macroscopic averaging ensuring ergodicity, where the former addresses the steady state statistics of the different queues employed at each device and the latter addresses the stochastic geometric network-wide performance. The simulation area is 5×5 km² with a wrapped-around boundaries to ensure unbiased statistics imposed by the network boundary devices. Unless otherwise stated, we consider the following physical layer parameters: $\kappa = 1$ (devices/BS/channel), $\eta = 4$, $\rho = \sigma^2 = -90$ and $N_c = 64$. For the MAC layer parameters, we consider three priority classes with $(\alpha_1, \alpha_2, \alpha_3) = (0.1, 0.25, 0.35)$ packets/slot, where all the queues have equal size (i.e., $k_1 = k_2 = k_3$).

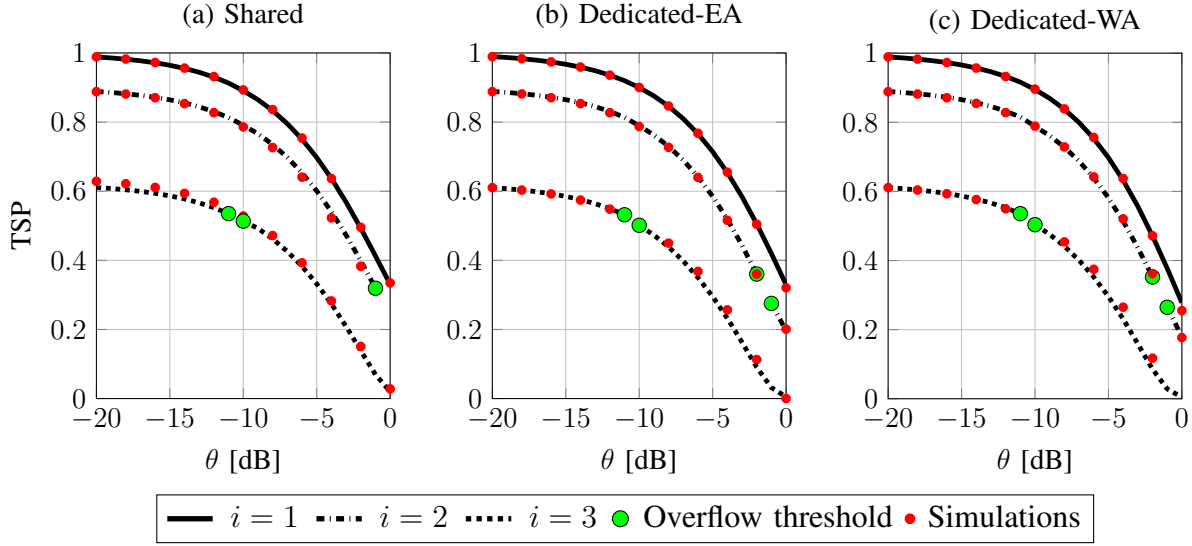


Fig. 5: Transmission success probability for the first three priority classes as a function of the SINR threshold θ . Three access strategies are shown (a) Shared (b) Dedicated-Equal allocation (c) Dedicated-Weighted allocation

Synchronous time-slotted system is adopted and each microscopic simulation run is considered as a time slot where independent channel gains are instantiated and packets are generated probabilistically. The queue occupancy for each of the considered priority classes are tracked. For a transition from one time slot to another, packets are independently generated at every simulated devices for all queues based on the batch arrival process (i.e., α_i). Every device with a non-empty queue of the N queues tries to communicate its backlogged packets with its serving BS based on the employed preemptive priority-aware transmission strategy. For a device with non-empty i -th priority queue, a packet is dispatched from the i -th priority queue if and only if i) all higher priority queues are empty, and ii) the achieved uplink SINR_i on the selected channel is greater than θ . In order to ensure that the different queues at the devices are in a steady state, simulation is first initiated with all queues at the devices as being idle and then it runs for a sufficiently high number of time slots until the steady-state is reached. Let $\hat{\mathbf{x}}^k = [\mathbf{x}_{1,0}^k, \mathbf{x}_{2,0}^k, \dots, \mathbf{x}_{N,0}^k]$ denotes the idle steady state probability for the t -th iteration of the N queues. Mathematically, the steady state is realized once $\|\hat{\mathbf{x}}^k - \hat{\mathbf{x}}^{k-1}\| < \epsilon$, where ϵ is some predetermined tolerance (e.g. 10^{-4}). After steady state is reached, all temporal statistics are then gathered based on sufficiently large number of microscopic realizations (i.e., 5000). Finally, the whole process is repeated for sufficiently large number of macroscopic network realizations (i.e., 10000) to ensure spatial ergodicity is reached.

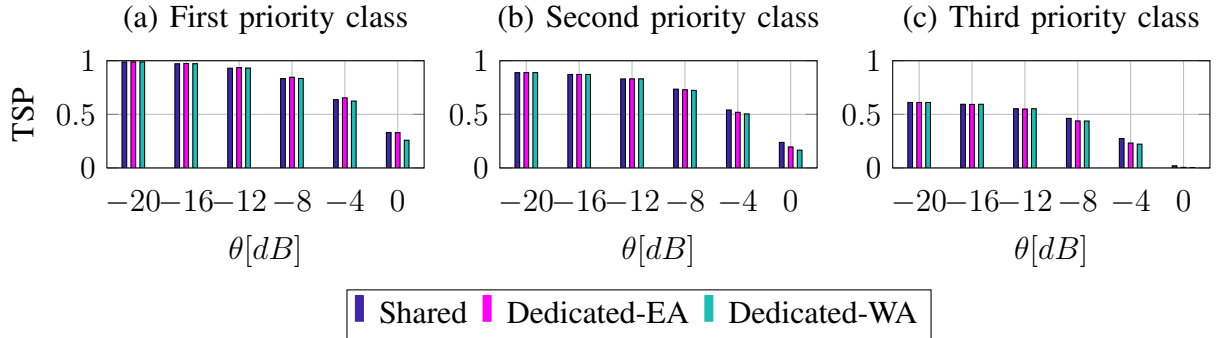


Fig. 6: Comparison of the three investigated access strategies for the three priority classes.

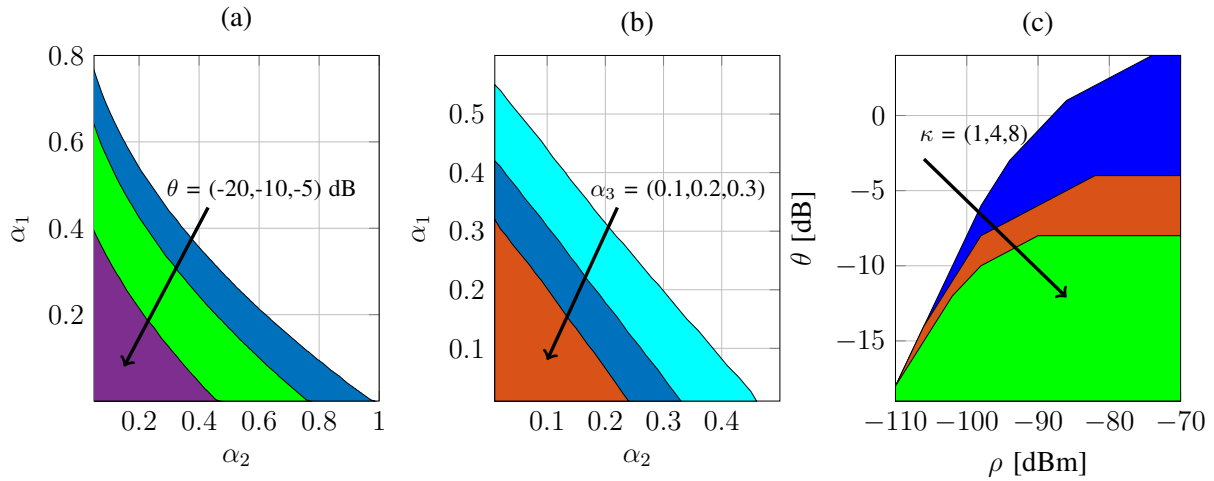


Fig. 7: Pareto frontiers for different system parameters.

B. Performance Evaluation

We start with the framework validation for all considered priority classes and access strategies. Fig. 5 shows the transmission success probability, as defined in (26), for the three priority classes with the shared, dedicated EA and WA against the SINR threshold θ . The close matching between the theoretical and simulation results validates the developed mathematical model. Note that the overflow thresholds depict the point where the probability of queues overflow starts to dominate. Focusing on a given access strategy and a priority class, the devices are able to empty their buffers and go into idle state when operating below the overflow threshold. This leads to a lower network aggregate interference. As θ increases, the service rate decreases, since the higher detection threshold reduces the probability of successful transmission attempts, which leads in turn into having higher aggregate network interference. Based on the adopted assumption that $\alpha_i > \alpha_j, \forall i < j$, it is expected that the transmission success probability for the i -th queue will be lower than that of the j -th queue. This is justified on the basis of the adopted priority-aware transmission, which implies that the lower priority packets are served, only if all the higher

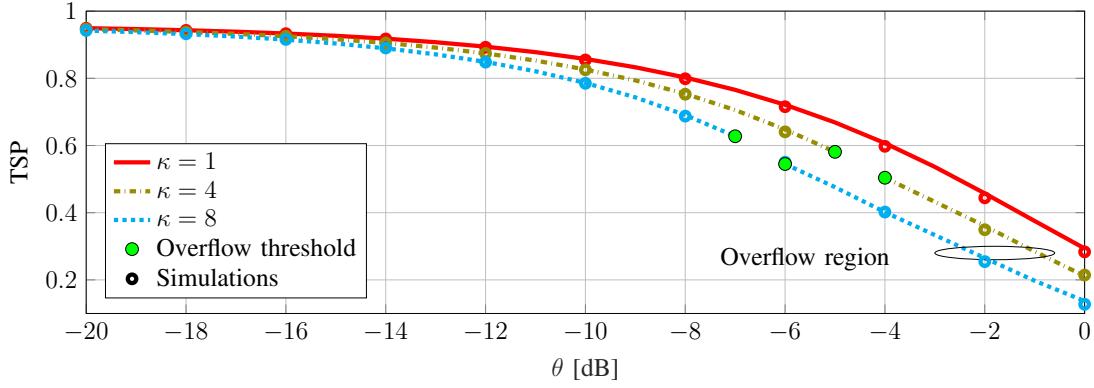


Fig. 8: Effect of devices densification on the first priority class.

priority queues are empty. In addition, it is clear that the threshold value θ , at which the system transitions from non-overflow to overflow operation depends on the priority class. Focusing on the different access strategies, it is observed that the shared access provides a larger non-overflow region for the second priority queue compared to the two other strategies.

In order to better assess the performance of the different strategies, Fig. 6 compares the three strategies. As mentioned earlier, the shared access strategy aims at allowing the devices to utilize all the available channels. Thus, a given device will have a larger pool of channels to utilize for its transmission, while facing larger portion of interfering active devices. On the other hand, the dedicated strategies imposes an allocation of the channels on the total number queues, either equally (i.e., EA) or proportionally (i.e., WA). This implies less number of channels is available, whilst interference from only active devices within the same priority class is existing. From Fig. 6, one can conclude that the shared access strategy is either providing similar performance or better for the investigated priority classes. This behavior can be interpreted via the head of queue effect of the higher priority packets. In the dedicated access strategy, when several devices have high priority packets, they keep interfering on a subset of the available channels leaving other channels for lower priority packets empty. In addition, the shared access strategy alleviates the required complexity to coordinate the channel allocation procedures for the dedicated strategies.

Fig. 7 shows the Pareto frontier for different system parameters that ensure queues operating below the overflow threshold, which is represented via the filled area under the curves. Note that only the shared access strategy is adopted in Fig. 7 for ease of visualization. First, Fig. 7(a) shows the relation between the arrival rates of the two highest priority classes (i.e., $i = 1, 2$) and the SINR threshold θ . As explained in Fig. 5, larger values of θ leads to increased aggregate network interference, thus, smaller non-overflow regions. Similarly, Fig. 7(b) highlights the effect

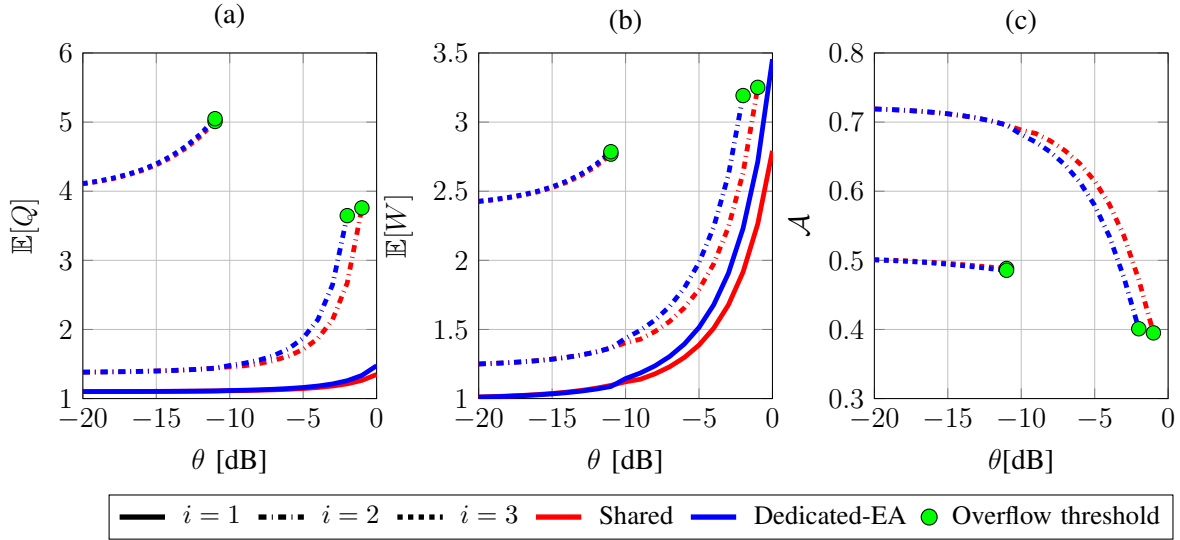


Fig. 9: Performance evaluation for shared and dedicated-equal allocation strategies (a) average number of packets (b) average transmission waiting time (c) service availability.

of considering different arrival rates of the third queue in the network. Due to the increased batch arrival rates, the overflow region decreases with larger arrival rates. Such a figure can provide interesting insights when studying the relation flow of different classes of traffic in order to ensure a stable network. Finally, Fig. 7(c) focuses on the relation between θ , uplink power control threshold ρ and devices intensity per BS per channel (i.e., κ). For a given κ , we can expect that as the uplink threshold gets higher, the feasible set of θ ensuring non-overflow operation increases till saturation is reached. This follows from the system transitioning from the noise limited to the interference limited scenario, which is governed by the value of σ^2 . On the other hand, as κ increases, the non-overflow region diminishes, which is due to the increased interference within the network.

Fig. 8 is considered to further study the effect of devices densification on the transmission success probability and network stability. As the value of κ increases, the typical queue experiences stronger interference which degrades the transmission success probability and shifts of the instability threshold to lower values of θ . Furthermore, the trade-off between increased number of employed channels (i.e., N_c) and enhanced performance can be observed. Thus, such a figure can help in deriving the minimum number of channels required to meet a targeted QoS.

In Fig. 9 different performance metrics are presented for the shared and dedicated EA strategies. The EA strategy is only selected in this assessment due to its close performance when compared to the WA strategy as shown in Fig. 6. First, Fig. 9(a) illustrates the average number

of packets for the three employed queues. It is observed that the shared strategy provides better performance when compared to the dedicated strategy for the first and second queue over all the investigated performance metrics. For the third queue, due to the deteriorated performance which results from the adopted priority-preemptive discipline, the both access strategies provide similar performance. Within a given access strategy, as the priority of the queue gets lower, its average number of packets increases which is justified from the adopted priority-based transmissions. Packets residing in a given queue will have to wait until all the higher queues are served, whilst new packets might arrive and accumulate in the queues. The figure also shows the effect of the queue's priority on the overflow threshold. Following a similar explanation, Fig. 9(b) demonstrates the average waiting time of a randomly selected packet within its queue. Such a metric is important when considering latency critical applications. The average waiting time depends on the packet's priority class and its service rate, which in turn depends on the aggregate network interference. Finally, the service availability is shown in Fig. 9(c). For the first priority class, such a metric equals one which is not shown. This is because packets belonging to the highest priority class will never experience vacation, thanks to the employed preemptive priority service discipline. As the priority gets lower, the service availability decreases, which is expected due to the priority-aware transmission strategy adopted. It can be concluded that the exclusive resource partitioning for prioritized grant-free uplink traffic in IoT systems provides lower performance compared to the shared access strategy.

VI. CONCLUSION

This paper presents a tractable and scalable spatiotemporal mathematical framework for massive uplink PMT IoT networks. Each device within the network accommodates a number of priority queues, generating packets, differentiated by their assigned priorities. Interactions between queues, in terms of the packet departure probabilities, occur due to aggregate network-wide mutual interference. Consequently, interdependency occurs between the microscopic (i.e., queues evolution) and macroscopic (aggregate network interference) scales. Tools from queueing theory are utilized to characterize the queues interaction within each device. Due to the adopted priority-aware transmission, service vacations occur within each device to lower priority packets to address higher priority packets. We propose a vacation-based queueing model that decomposes the different priority queues at each device to a single-queue system with server vacation. Employing such a vacation-based queueing model offers a tractable and scalable alternative to conventional

state of the art, which are hindered by the curse of dimensionality problem. Furthermore, we utilize stochastic geometry to account for the network-wide aggregate interference. To this end, an iterative algorithm is proposed that aims at characterizing the steady state probabilities and the coverage probabilities for the different priority classes. In addition, we consider two channel access strategies; namely dedicated and shared. For the former strategy, an IoT device randomly and uniformly selects one of the channels dedicated for the addressed packet priority. On the other hand, an IoT device in the shared strategy randomly and uniformly selects one of the complete set of channels regardless of the packet priority. Based on the transmission success probability, average number of packets within a queue, average waiting time and service availability, shared access strategy shows better performance when employed in large scale grant-free uplink IoT networks. As a result, resource allocation on a traffic level for grant-free IoT systems provides lower performance compared to the shared access strategy. Finally, we show different insights on the scalability and overflow conditions of the network, which defines the network parameters at which the network can serve all packets generated by the IoT devices without dropping newly incoming packets.

APPENDIX A

PROOF OF LEMMA 1

In order to fully characterize the vacation period for a given priority class, one needs to first determine the busy period of the higher priority queues. For the highest priority class (i.e., $i = 1$), with queue size k_1 , its transition matrix P_1 is that of a simple birth-death process. Additionally, its busy period, denoted as \mathbf{V}_1 is represented via the following absorbing Markov chain

$$\mathbf{V}_1 = \begin{bmatrix} \bar{\alpha}_1 \bar{p}_1 + \alpha_1 p & \alpha_1 \bar{p}_1 & & & \\ \bar{\alpha}_1 p & \bar{\alpha}_1 \bar{p}_1 + \alpha_1 p & \alpha_1 \bar{p}_1 & & \\ & & \ddots & \ddots & \\ & & & \bar{\alpha}_1 p & \bar{\alpha}_1 \bar{p}_1 + \alpha_1 p \end{bmatrix}. \quad (30)$$

Let $\tilde{\mathbf{v}}_1 \in \mathbb{R}^{k_1-1 \times 1}$ denotes the absorption vector, which is $\tilde{\mathbf{v}}_1 = [\bar{\alpha}_1 p_1 \ \mathbf{0}_{k_1}]$. Through \mathbf{V}_1 and $\tilde{\mathbf{v}}_1$, one can fully characterize the transitions when a first priority packet arrives as well as its successful departure (i.e., absorption). Accordingly, the second priority queue can be modeled as Geo/PH/1 queue, where the PH type distribution models the busy period of the first priority queue. Consider then the case of serving second priority packets, if a first priority packet arrives, an initialization vector \mathbf{v}_1 is required to characterize the states distribution as well as the probability

of their occurrence χ_1 . Such a vector equals $\mathbf{v}_1 = [1 \ \mathbf{0}_{k_1}]^T$, since the queue is initialized as empty and $\chi_1 = \alpha_1$. The analysis for a general i -th priority class is then derived and with some algebraic operations, the lemma is finalized.

APPENDIX B

PROOF OF THEOREM 1

For the dedicated access scheme, a packet belonging to the i -th queue will only experience aggregate interference from packets belonging to the same priority class. Such a packet will be granted transmission only if its respective queue is not empty and all the higher queues are empty. Consequently, the set of interfering device for the i -th queue at the typical BS is $\mu\zeta_i$, where $\zeta_i = \sum_{z_i=1}^{k_i} \mathbf{x}_{(1,0),(2,0),\dots,(i-1,0),(i,z_i)}$ is the joint probability of having idle $i-1$ queues and non-idle i -th queue. The adopted grant-free (i.e., unscheduled) transmission scheme among the devices imposes a differentiation between the experienced interference into intra-cell and inter-cell interference, thus (21) is written as

$$p = \exp\left\{-\frac{\sigma^2\theta}{\rho}\right\} \mathcal{L}_{I_{\text{out}}}\left(\frac{\theta}{\rho}\right) \mathcal{L}_{I_{\text{in}}}\left(\frac{\theta}{\rho}\right). \quad (31)$$

Since a full channel inversion power control with threshold ρ is employed, two main results hold: (i) Received power from the devices at a given BS equals ρ (ii) Interference power from the neighboring devices is strictly lower than ρ . Following [24], the aggregate inter-cell interference at the serving BS for the i -th priority queue is

$$\mathcal{L}_{I_{\text{out}}}(s) \approx \exp\left(-2\pi x_{(1:N,0)} \mu s^{\frac{2}{\eta}} \mathbb{E}_P\left[P^{\frac{2}{\eta}}\right] \int_{(s\rho)^{\frac{1}{\eta}}}^{\infty} \frac{y}{y^n + 1} dy\right). \quad (32)$$

The inter-cell interference follows that of [19, Lemma 1], as

$$I_{\text{in}} = \mathbb{P}\{\mathcal{N} = 0\} + \sum_{n=1}^{\infty} \frac{\mathbb{P}\{\mathcal{N} = n\}}{(1 + s\rho)^n}, \quad (33)$$

where \mathcal{N} is a random variable representing the number of neighbors. Plugging (32) and (33) into (31) and following [19, Lemma 1], the theorem is derived.

APPENDIX C

PROOF OF THEOREM 2

Due to the adopted shared access strategy between the different priority classes along with the vacation-based model, p_i of all the queues are identical, since each queue experiences the same aggregate interference (i.e., $p_i = p_j = p, \forall i, j \in \{1, 2, \dots, N\}, i \neq j$). The set of interfering

device for the i -th queue at the typical BS is $\mu\bar{x}_{(1:i,0)}$. Finally, the lemma is shown following similar steps as Theorem 1.

REFERENCES

- [1] A. Al-Fuqaha, M. Guizani, M. Mohammadi, M. Aledhari, and M. Ayyash, "Internet of things: A survey on enabling technologies, protocols, and applications," *IEEE Communications Surveys Tutorials*, vol. 17, no. 4, pp. 2347–2376, Fourthquarter 2015.
- [2] 3GPP, "TS 22.261 service requirements for next generation new services and markets," *3rd Generation Partnership Project (3GPP)*, v16.3.0, 2018.
- [3] —, "TR 36.746 study on further enhancements to LTE device to device, user equipment to network relays for internet of things and wearables," *3rd Generation Partnership Project (3GPP)*, v15.1.1, 2018.
- [4] W. Ayoub, A. E. Samhat, F. Nouvel, M. Mroue, and J. Prvotet, "Internet of mobile things: Overview of LoRaWAN, DASH7, and NB-IoT in LPWANs standards and supported mobility," *IEEE Communications Surveys Tutorials*, pp. 1–1, 2018.
- [5] NGMNA, "Recommendations for NGMN KPIs and requirements for 5G," *Next Generation Mobile Networks Alliance*, 2016.
- [6] A. Bader, H. ElSawy, M. Gharbieh, M. Alouini, A. Adinoyi, and F. Alshalan, "First mile challenges for large-scale IoT," *IEEE Communications Magazine*, vol. 55, no. 3, pp. 138–144, March 2017.
- [7] G. Berardinelli, N. Huda Mahmood, R. Abreu, T. Jacobsen, K. Pedersen, I. Z. Kovcs, and P. Mogensen, "Reliability analysis of uplink grant-free transmission over shared resources," *IEEE Access*, vol. 6, pp. 23 602–23 611, 2018.
- [8] 3GPP, "TS 23.203 policy and charging control architecture," *3rd Generation Partnership Project (3GPP)*, v16.0.0, 2019.
- [9] IEEE, "802.1Qbv-enhancements for scheduled traffic," *Institute of Electrical and Electronics Engineers, Inc*, 2016. [Online]. Available: <http://www.ieee802.org/1/pages/802.1bv.html>
- [10] 5G-ACIA, "5G for connected industries and automation," *5G Alliance for Connected Industries and Automation*, 2018.
- [11] H. Ekstrom, "Qos control in the 3GPP evolved packet system," *IEEE Communications Magazine*, vol. 47, no. 2, pp. 76–83, February 2009.
- [12] D. A. Chekired, L. Khoukhi, and H. T. Mouftah, "Industrial IoT data scheduling based on hierarchical fog computing: A key for enabling smart factory," *IEEE Transactions on Industrial Informatics*, vol. 14, no. 10, pp. 4590–4602, Oct 2018.
- [13] S. Craciunas, R. Serna Oliver, M. Chmelk, and W. Steiner, "Scheduling real-time communication in IEEE 802.1Qbv time sensitive networks," in *24th International Conference on Real-Time Networks and Systems*, 2016.
- [14] L. Zhao, P. Pop, and S. S. Craciunas, "Worst-case latency analysis for IEEE 802.1Qbv time sensitive networks using network calculus," *IEEE Access*, vol. 6, pp. 41 803–41 815, 2018.
- [15] J. G. Andrews, F. Baccelli, and R. K. Ganti, "A tractable approach to coverage and rate in cellular networks," *IEEE Transactions on Communications*, vol. 59, no. 11, pp. 3122–3134, November 2011.
- [16] H. ElSawy, E. Hossain, and M. Haenggi, "Stochastic geometry for modeling, analysis, and design of multi-tier and cognitive cellular wireless networks: A survey," *IEEE Communications Surveys Tutorials*, vol. 15, no. 3, pp. 996–1019, Third 2013.
- [17] H. ElSawy, A. Sultan-Salem, M. Alouini, and M. Z. Win, "Modeling and analysis of cellular networks using stochastic geometry: A tutorial," *IEEE Communications Surveys Tutorials*, vol. 19, no. 1, pp. 167–203, Firstquarter 2017.
- [18] Y. Zhong, T. Q. S. Quek, and X. Ge, "Heterogeneous cellular networks with spatio-temporal traffic: Delay analysis and scheduling," *IEEE Journal on Selected Areas in Communications*, vol. 35, no. 6, pp. 1373–1386, June 2017.

- [19] M. Gharbieh, H. ElSawy, A. Bader, and M. Alouini, "Spatiotemporal stochastic modeling of IoT enabled cellular networks: Scalability and stability analysis," *IEEE Transactions on Communications*, vol. 65, no. 8, pp. 3585–3600, Aug 2017.
- [20] M. Gharbieh, H. ElSawy, H. Yang, A. Bader, and M. Alouini, "Spatiotemporal model for uplink IoT traffic: Scheduling and random access paradox," *IEEE Transactions on Wireless Communications*, vol. 17, no. 12, pp. 8357–8372, Dec 2018.
- [21] H. H. Yang and T. Q. S. Quek, "Spatiotemporal analysis for SINR coverage in small cell networks," *IEEE Transactions on Communications*, pp. 1–1, 2019.
- [22] G. Chisci, H. ElSawy, A. Conti, M. Alouini, and M. Z. Win, "Uncoordinated massive wireless networks: Spatiotemporal models and multiaccess strategies," *IEEE/ACM Transactions on Networking*, pp. 1–14, 2019.
- [23] A. S. Alfa, *Applied discrete-time queues, second edition*. Springer-New York USA, 01 2015.
- [24] H. ElSawy and E. Hossain, "On stochastic geometry modeling of cellular uplink transmission with truncated channel inversion power control," *IEEE Transactions on Wireless Communications*, vol. 13, no. 8, pp. 4454–4469, Aug 2014.
- [25] F. Machihara, "A preemptive priority queue as a model with server vacations," *Journal of the Operations Research Society of Japan*, vol. 39, no. 1, pp. 118–131, 1996.
- [26] M. V. Vuuren and I. Adan, "Approximate analysis of general priority queues," in *Analysis of manufacturing systems*, 2007.
- [27] A. Slepchenko, J. Selen, I. Adan, and G.-J. van Houtum, "Joint queue length distribution of multi-class, single-server queues with preemptive priorities," *Queueing Systems*, vol. 81, no. 4, pp. 379–395, Dec 2015. [Online]. Available: <https://doi.org/10.1007/s11134-015-9460-z>
- [28] V. G. Kulkarni, "Introduction to matrix analytic methods in stochastic modeling, by g. latouche and v. ramaswamy," *Journal of Applied Mathematics and Stochastic Analysis*, vol. 12, 01 1999.
- [29] R. M. Loynes, "The stability of a queue with non-independent inter-arrival and service times," *Mathematical Proceedings of the Cambridge Philosophical Society*, vol. 58, no. 3, p. 497520, 1962.
- [30] I. Krikidis, T. Charalambous, and J. S. Thompson, "Buffer-aided relay selection for cooperative diversity systems without delay constraints," *IEEE Transactions on Wireless Communications*, vol. 11, no. 5, pp. 1957–1967, May 2012.
- [31] H. Y. Lee, Y. J. Sang, and K. S. Kim, "On the uplink SIR distributions in heterogeneous cellular networks," *IEEE Communications Letters*, vol. 18, no. 12, pp. 2145–2148, Dec 2014.
- [32] M. Haenggi, "The meta distribution of the sir in poisson bipolar and cellular networks," *IEEE Transactions on Wireless Communications*, vol. 15, no. 4, pp. 2577–2589, April 2016.
- [33] H. ElSawy and M. Alouini, "On the meta distribution of coverage probability in uplink cellular networks," *IEEE Communications Letters*, vol. 21, no. 7, pp. 1625–1628, July 2017.
- [34] Y. Wang, M. Haenggi, and Z. Tan, "The meta distribution of the sir for cellular networks with power control," *IEEE Transactions on Communications*, vol. 66, no. 4, pp. 1745–1757, April 2018.
- [35] M. Haenggi, *Stochastic Geometry for Wireless Networks*. New York, NY, USA: Cambridge University Press, 2012.
- [36] Y. Zhou and W. Zhuang, "Performance analysis of cooperative communication in decentralized wireless networks with unsaturated traffic," *IEEE Transactions on Wireless Communications*, vol. 15, no. 5, pp. 3518–3530, May 2016.